Ganymede's atmosphere as constrained by HST/STIS observations

F. Leblanc[1], Roth L.[2], Chaufray J.Y.[1], R. Modolo[1], M. Galand[3], N. Ivchenko[2], G. Carnielli[3], C. Baskevitch[1], A. Oza[4] and A.L.E. Werner[1, 5]

[1] LATMOS/CNRS, Sorbonne Université, UVSQ, Paris, France

[2] Space and Plasma Physics, KTH Royal Institute of Technology, Stockholm, Sweden

[3] Department of Physics, Imperial College London, London, UK

[4] Jet Propulsion Laboratory, California Institute of Technology, Pasadena, USA

[5] Now at Swedish Institute of Space Physics, Uppsala, Sweden

Abstract

A new analysis of aurora observations of Ganymede's atmosphere on the orbital leading and trailing hemispheres has been recently published by Roth et al. (2021), suggesting that water is its main constituent near noon. Here, we present two additional aurora observations of Ganymede's sub-Jovian and anti-Jovian hemispheres, which suggest a modulation of the atmospheric H_2O/O_2 ratio on the moon's orbital period, and analyze the orbital evolution of the atmosphere. For this, we propose a reconstruction of aurora observations based on a physical modelling of the exosphere taking into account its orbital variability (the Exospheric Global Model; Leblanc et al. 2017). The solution described in this paper agrees with Roth et al. (2021) that Ganymede's exosphere should be dominantly composed of water molecules. From Ganymede's position when its leading hemisphere is illuminated to when it is its trailing hemisphere, the column density of O_2 may vary between 4.3×10^{14} and 3.6×10^{14} cm^{-2} whereas the H_2O column density should vary between 5.6×10^{14} and 1.3×10^{15} cm^{-2}. The water content of Ganymede's atmosphere is essentially constrained by its sublimation rate whereas the O_2 component of Ganymede's atmosphere is controlled by the radiolytic yield. The other species, products of the water molecules, vary in a more complex way depending on their sources, either as ejecta from the surface and/or as product of the dissociation of the other atmospheric constituents. Electron impact on H_2O and H_2 molecules is shown to likely produce H Lyman-alpha emissions close to Ganymede, in addition to the observed extended Lyman-alpha corona from H resonant scattering. All these conclusions being highly dependent on our capability to accurately model the origins of the observed Ganymede auroral emissions, modelling these emissions remains poorly constrained without an accurate knowledge of the Jovian magnetospheric and Ganymede ionospheric electron populations.

I Introduction

As summarized in Roth et al. (2022), only very few direct observations of Ganymede's atmosphere have been realized so far. The very first evidence of Ganymede's atmosphere was obtained by Galileo FUV instrument in 1996 (Barth et al. 1997) and revealed an extended atmosphere of H atoms, an observation later confirmed by the Space Telescope Imaging Spectrograph of the Hubble Space Telescope (HST/STIS; Feldman et al. 2000; Alday et al. 2017). Alday et al. (2017) concluded that the Lyman α emission brightness does not vary along Ganymede's orbit with an average corona emission intensity of ~320 R corresponding to a column density of $1.55\pm1.2\times10^{12}$ H/cm² if only produced by resonant scattering. Recent HST/STIS observations of Ganymede in transit (Roth et al. 2023) found weak but widely extended absorption around the moon, confirming the H corona profile and densities derived earlier. In 1996, the Goddard High Resolution Spectrograph of the Hubble Space Telescope (HST/GHRS) obtained the first evidence of two other emission lines at 130.4 and 135.6 nm from Ganymede's atmosphere (Hall et al. 1998). The ratio of these two emissions strongly suggested that these observed emissions were probably due to electron impact on O_2 molecules. Moreover, the first images of these emission lines obtained by HST/STIS clearly showed that the 135.6 nm was confined in the polar regions (Hall et al. 1998) and even roughly colocated to the open-closed field line boundary (OCFB) of Ganymede magnetosphere (McGrath et al. 2013; Molyneux et al. 2018). The auroral nature of these two emissions implies that their brightnesses depend essentially on three parameters: the column density and composition of the neutral atmosphere and the energy flux distribution of the electrons. When supposing that the observed emission was only produced by electron impact on O_2, without a knowledge of the electron distribution in these regions, the column density of O_2/cm^2 could not be estimated very accurately and was inferred to be between 10^{14} to 10^{15} O_2/cm^2 (Hall et al. 1998; Molyneux et al. 2018). No observation constraining the H_2O, OH and H_2 exosphere of Ganymede has been obtained up to Roth et al. (2021), whereas the oxygen atomic species was tentatively identified (Molyneux et al. 1998; Roth et al. 2021).

Considering the relatively limited number of observations and the difficulty to realize new ones, modelling Ganymede's atmosphere remains presently our best approach to get an idea on how this atmosphere might be spatially organized and temporarily variable. This atmosphere is thought to be essentially composed of H_2O, O_2 and their products. H_2O is essentially produced by sublimation near the subsolar point, which according to Marconi (2007), Shematovitch (2016) and Leblanc et al. (2017) leads to a partially surface bounded exosphere in reference to the Moon exosphere (Stern 1999). But H_2O can also be produced by the sputtering of Ganymede icy surface (Cassidy et al. 2013) at high latitudes.

Our ability to model Ganymede's atmosphere depends therefore on several parameters:

- the surface temperature and composition (Spencer et al. 1989; Leblanc et al. 2017),

- the spatial dependency of the ion bombardment of the surface by the Jovian particles (Plainaki et al. 2020a, b; Vorburger et al. 2022) but also by ions produced locally in Ganymede's neutral atmosphere (Carnielli et al. 2020b),

- the ejection rate induced by the sputtering (Cooper et al. 2001; Turc et al. 2014; Plainaki et al. 2015; 2020a, b and Carnielli et al. 2020a, b) and by sublimation (Johnson et al. 1989; Fray and Schmitt 2009; Leblanc et al. 2017; Vorburger et al. 2022),

- the losses by photon and electron ionization and dissociation, as well as by reabsorption at the surface and by neutral and ion escape,

- the orbital variability of all these parameters (Plainaki et al. 2015; Leblanc et al. 2017).

Recently, Roth et al. (2021) proposed an original analysis of new and old HST/STIS observations obtained at two different orbital positions of Ganymede. These authors suggested that the radial distribution of the 130.4 nm and 135.6 nm emission lines brightness was consistent with the existence of a dominant H_2O atmospheric component and with its predicted orbital variability. Based on a simple symmetric model of the atmosphere, Roth et al. (2021) concluded that Ganymede's

atmosphere water column density peaks at a value of 6×10^{15} H_2O/cm^2 near the center of the visible disk when the trailing hemisphere is illuminated, a value which decreases to 1×10^{15} H_2O/cm^2 when the leading hemisphere of Ganymede is illuminated.

In the following, we present a detailed comparison between these observations and the results of simulation performed with Exospheric Global Model, EGM (Leblanc et al. 2017; Oza et al. 2019). In section II, we briefly describe the set of observations analyzed in this paper, in section III, our model, whereas in section IV a detailed comparison and discussion of the main lessons from such a comparison are provided. Section V summarizes the main conclusions of this work.

II HST/STIS Observations

Roth et al. (2021) reported the first indirect observation of Ganymede water atmosphere. They used two sets of images by Hubble's Space Telescope Imaging Spectrograph (HST/STIS) performed at two positions of Ganymede along its orbit:

- at a phase angle of 98° - 111° (2010-11-19, Figure 1 in yellow), that is with the leading hemispheric side of Ganymede being illuminated,

- at a phase angle of 289° - 300° (1998-10-30, Figure 1 in blue), that is with the trailing hemispheric side of Ganymede being illuminated.

In addition, Roth et al. (2021) analyzed spectra taken with HST's Cosmics Origins Spectrograph (COS) at a phase angle of 352° – 357°, that is just before and partly when Ganymede is in the shadow of Jupiter. At such phase angle, they reported no significant change in the relative intensity of the two oxygen lines, 130.4 and 135.6 nm, suggesting that the atomic oxygen atmospheric content should not exceed 2×10^{12} O/cm^2. In the following, we will not use the COS spectra in our analysis because these observations were only used to estimate an upper limit for the exospheric content in atomic oxygen and do not provide useful spatial information on the emissions.

To the two sets of HST/STIS observations, we add two other sets of HST/STIS observations obtained at two complementary positions of Ganymede (Figure 1; Marzok et al. 2022):

- at a phase angle of 173-177° obtained with STIS on the 02/02/2017 (Figure 1, in green),

- at a phase angle of 335°-340° obtained with STIS on the 11/30/2003 (Figure 1, in red).

These two later sets of observations nicely complete the ones described in Roth et al. (2021) even if obtained with lower signal/noise ratio (Figure 2) and allow us to track the atmospheric orbital variability. The 135.6 nm images have been published in McGrath et al. (2013) (2003 dataset) and Marzok et al. (2022) (2017 dataset). For this study, the 130.4 images obtained simultaneously were analyzed for the first time and are used in addition. The data processing and image analysis of the new datasets follows the same steps as described in Roth et al. (2021), Roth et al. (2016) and (2014):

- Earth 130.4 nm Geocorona is taken into account by selecting low-Geocorona exposures when HST was in Earth's nightside and by monitoring the 130.4 nm background signal as HST moves into Earth's shadow (Roth et al. 2016). The background induced by the Geocorona, interplanetary medium and torus emissions is also estimated and subtracted using two regions far from Ganymede disk along the slit (Roth et al. 2014).

- Solar reflected light from Ganymede's surface (surface albedo) is subtracted from the observation using UV daily observations by SORCE/SOLSTICE instrument (McClintock et al. 2005) taking into account STIS G140L resolution and using a homogeneous bright model disk of Ganymede convolved with STIS Point Spread Function and adjusted to match the observed surface reflection signal between 143 and 153 nm. We have tested different phase angle dependencies for the surface reflection between a uniform disk (as used in Roth et al. 2021) and a Lambertian reflector using the description from Oren and Nayar (1994). The effects on the resulting emission ratio is less than 10% and for the presented results we used the simple uniform disk reflectance.

From the corrected HST/STIS images, we calculated the radial profiles of the intensity of the 130.4 and 135.6 nm emissions by integrating its brightness on annulus centred on Ganymede's disk and binned in steps of 0.2 R_G for the observations obtained at a phase angle of 98°-111° and 298°-300° (panels a and d in Figure 2), of 0.4 R_G for a phase angle of 335°-340° (panel b in FIgure 2) and of 0.25 R_G for a phase angle of 173°-177° (panel c in Figure 2). The large bin size in panel b is chosen to get somewhat lower error bars while still keeping a reasonable number of 4 bins to actually see a radial profile trend.

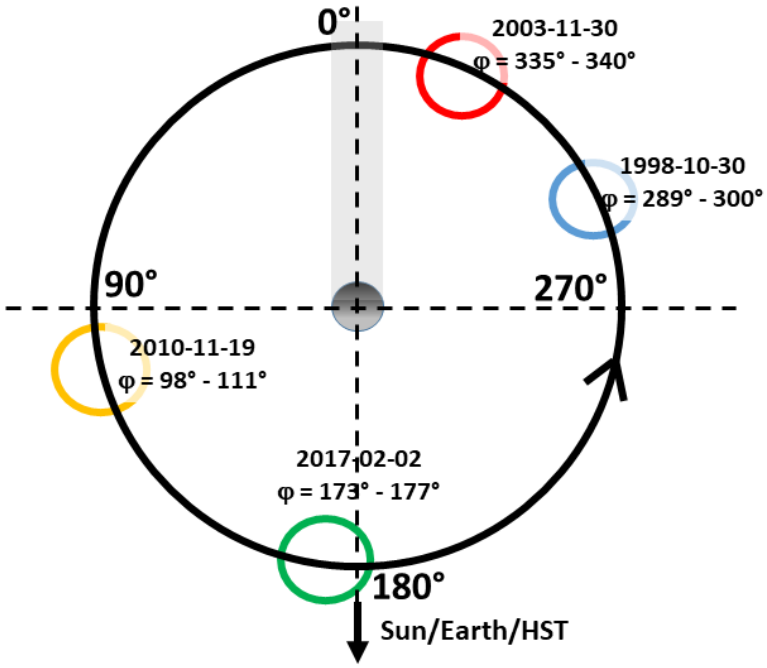

Figure 1: *Positions of Ganymede during the four sets of observations of HST/STIS used in this paper. We also indicated the range of phase angle of each set of observations as well as their date. The caption colors of the circle refer to Figures 2 and 6.*

Figure 2 provides a view of the four sets of observations used in this paper. At the four orbital positions of Ganymede (Figure 1), HST/STIS realized 2D images of the emission brightness intensity of the 130.4 nm and 135.6 nm emission lines (left panels of each set of observations) from which it was

147 possible to extract an average emission intensity profile with respect to the distance from the center
148 of Ganymede apparent disk (right top panel). We also derived the ratio of these two emissions lines
149 as a function of the distance from the center (right bottom panels). This ratio is displayed up to 1.4 R_G
150 whereas the 2D images show pixels up to at least 1.2 R_G (panel d). The observations use a long slit
151 and the images therefore do not go beyond the left and right edges shown in Figure 2, but above and
152 below the displayed images. However, because the signal-to-noise ratio of a single pixel is well below
153 1 at distances > 1.2 R_G, we choose not to show those pixels above 1.2 R_G in these 2D images. When
154 the signal was low, we rather choose to integrate over few pixels to show a significant signal, not
155 necessarily showing the noisy spatially resolved data. As explained in Roth et al. (2021) and displayed
156 in Figure 3d, this ratio should be of ~2.3 if both emissions are produced by the electron impact on O_2
157 only. The ratio is close to ~0.2 if produced by electron impact on H_2O and is lower than 0.1 if
158 produced by electron impact on atomic O (Figure 3d).

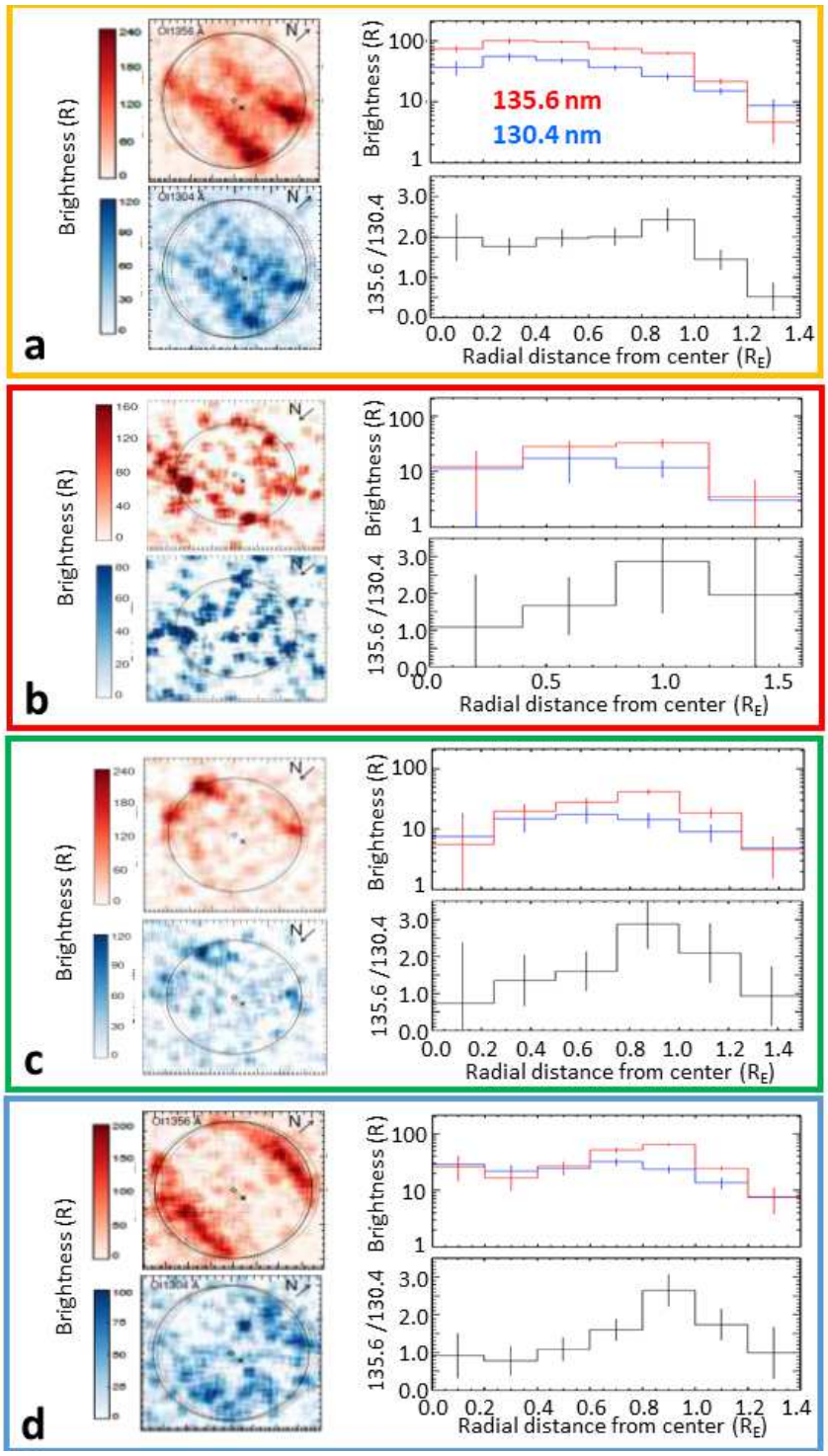

Figure 2: *Observation of Ganymede's atmospheric emission by HST/STIS. Each panel corresponds to one position displayed in Figure 1: a 2010-11-19, phase angle of 98°-111° (Roth et al. 2021). b: 2003-11-30, phase angle of 335°-340° (McGrath et al. 2013). c: 2017-02-02, phase angle of 173° - 177°. d: 1998-10-30, phase angle between 289° - 300° (Roth et al. 2021). Each panel surrounded by a rectangle whose colour corresponds to that used for the circles in Figure 1 is composed of the STIS*

images of the 135.6 nm (red) and 130.4 nm (blue) brightness intensities, of the radial profile from the center of the disk up to around half a radius above the limb of the emission brightness intensity at these two wavelengths (top right panel in each rectangle where the red solid line corresponds to the 135.6 nm emission brightness and the blue solid line to the 130.4 nm emission brightness) and of the ratio of the 135.6 nm emission intensity divided by the 130.4 nm emission intensity (bottom right panel in each rectangle). The North direction in panels b and c (pointing towards the bottom of the figure) is inverted with respect to the North direction in panels a and b (pointing towards the top of the figure).

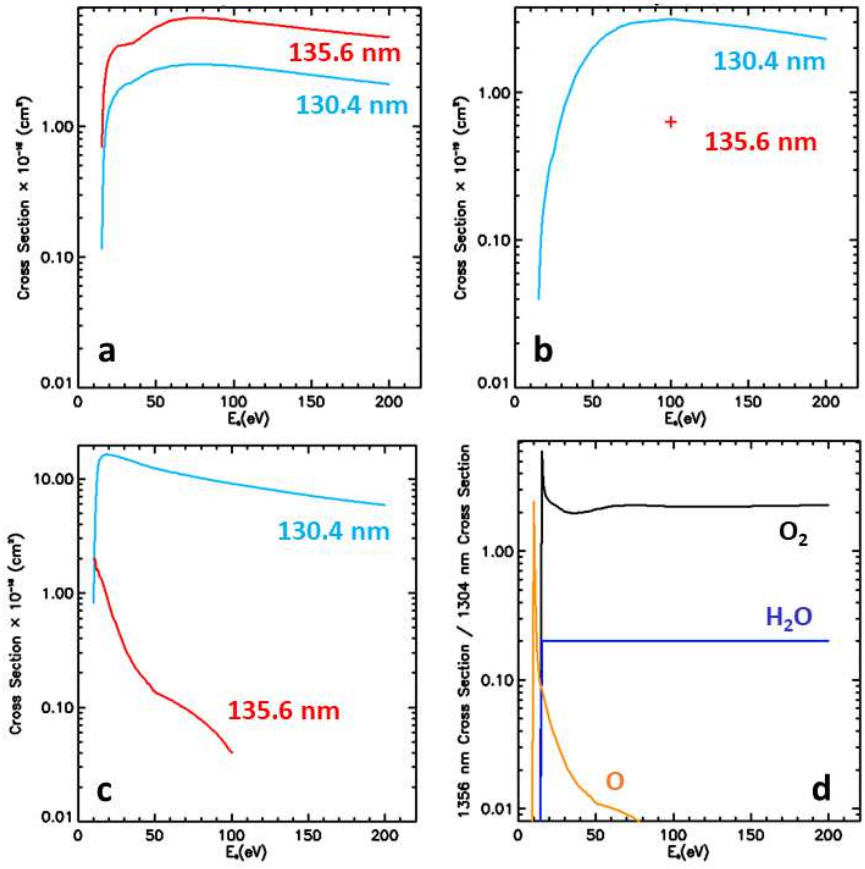

Figure 3: *Emission excitation electron impact cross sections. a: O_2 + e (Kanik et al. 2003). b: H_2O + e (Makarov et al. 2004) and only available measurement of the H_20 + e 135.6 nm at 100 eV (Roth et al. 2021). c: O + e (Tayal et al. 2016 for 135.6 nm; Johnson et al. 2005 for 130.4 nm). d: ratio of the 135.6 nm / 130.4 nm emission excitation cross section for O_2+e (black line), H_2O+e (blue line, with the*

178 *assumption that the only measurement at 100 eV is valid on the whole range of electron energy*
179 *plotted here) and O+e (orange line).*

180

181 As displayed in Figure 2, the observed ratio of the 135.6 nm / 130.4 nm emission line brightness
182 varies between 3.0 and 0.5 and was interpreted as a signature of the mixture of H_2O or O relative to
183 O_2. Roth et al. (2021) also suggested that the contribution to these emission lines from electron
184 impact on atomic oxygen was negligible on the disk but can explain the observed decrease in the
185 135.6 nm / 130.4 nm ratio above the limb (at radial distance > 1 R_G in Figure 2).

186 As shown in Figure 2, the best observations in terms of signal noise ratio were obtained when
187 Ganymede was at a phase angle of 98° - 111° (panel a) and 289° - 300° (panel d) (Roth et al. 2021).
188 Adding two other sets of observation allow us to highlight the orbital variability of Ganymede's
189 atmosphere. The 135.6 nm / 130.4 nm emission intensity ratio at the center of the disk (all pixels
190 inside < 0.5 R_G) is lower than ~1.0 at a phase angle of *289° - 300°* (panel d), i.e. when the trailing
191 hemisphere is observed. It is slightly higher with values around 1-1.5 on the subjovian (335°- 340°,
192 panel b) and antijovian sides (173°-177°, panel c) and peaking at a value around 2.0 at a phase angle
193 of 98° - 111° (panel a, wake or leading hemisphere). If interpreted with the H_2O abundance reducing
194 the ratio, the observations of a systematically lower ratio at the four orbital positions implies that the
195 H_2O atmosphere is not transient but constantly present. The value of the oxygen emission ratio is
196 around 2.5 at the limb at all four orbital positions.

197 We note that the propagated uncertainty of the OI ratio near the disk center in the profiles of the
198 newly added images is particularly high, allowing in principle for values consistent with (almost) only
199 O_2 in the atmosphere. However, when integrating all pixels within 0.8 R_G for the phase angle 335°-
200 340° images (panel b, corresponding to the first 2 radial bins), we find a OI ratio of 1.4 ± 0.8 , which is
201 slightly outside the 1-sigma bounds for a pure O2 atmosphere. Integrating over all pixels withing 0.6
202 R_G for the phase angle 173° - 177° image (panel c, ~2.4 bins), the OI ratio of 1.1 ± 0.5 is inconsistent

with pure O_2 at a 2-sigma level. Thus, also only marginally significant, the radial trend in the OI ratio found by Roth et al. (2021) is also present in the new two datasets.

The 2D images of the emission brightness might help us to explain this variability, with auroral regions closer to the center of the disk at 98° - 111° and 173° - 177° than at 289° - 300° and 335° - 340°. As shown in Marconi (2007), Ganymede's atmosphere is probably composed of H_2O and O_2 and of their products, with a denser O_2 atmosphere in the polar auroral regions and an H_2O atmosphere essentially produced by sublimation around the subsolar region. In another way, at phase angles of 98° - 111°, the auroral regions are close to the center of the apparent disk, that is, to a region dominated by H_2O leading to a low ratio of the two O emission lines. At 177°, the auroral regions are close to the limb far from the subsolar region, in a region of the exosphere dominated by O_2 leading to a higher ratio of these two O emission lines.

In order to properly compare observation and simulation, there are three effects that should be considered because they can degrade the spatial resolution when observing Ganymede with HST/STIS:

- the pixel resolution of the instrument which is about 80 km,
- the PSF-smearing of about 2-2.5 pixels,
- the spectral smearing due to the dispersion included in the telescope setup. This will be small and not distinguishable from spatial effects. We neglect the effects in our modelling.

The first two effects are taken into account by projecting the simulated image on a grid with 80 km resolution and then convolving this with a 2D Lorentzian with a FWHM of 2.5 pixels.

III Exospheric Global Model

III.1 Description of the model

The Exospheric Global Model (EGM) is a 3D time dependent Monte Carlo model that describes the fate of atmospheric species ejected from Ganymede's surface, moving under the influence of Ganymede and Jupiter gravity fields, being absorbed or reejected when reimpacting the surface and eventually ionized or dissociated by photon and electron impacts. All products of water and O_2 are described, that is, H_2O, H, H_2, O, O_2 and OH. EGM can also describe the effects of collision between these species in the case of weakly dense atmosphere but in the following we will present simulations performed by neglecting collisions between atmospheric species. Indeed, as explained in Leblanc et al. (2017), collisions have a limited impact on the 3D large scale structure of the atmosphere and would not change the conclusions of this present work. All details regarding EGM can be found in Leblanc et al. (2017). EGM is time dependent so that it allows to follow the trajectory of the exospheric particles all along Ganymede rotation around Jupiter. It therefore takes into account the centrifugal and Coriolis forces applied on these particles due to Ganymede rotation in Jupiter frame and the variations of the solar illumination (including the shadow induced by Jupiter) during Ganymede's orbit.

With EGM, we reconstruct in 3D the density, bulk velocity and temperature of all neutral species around Ganymede. In order to reconstruct the emission intensity, we consider the various electron and photon induced reactions that could produce the 130.4 nm, 135.6 nm or 121.6 nm emissions. In the case of electron impact induced emission excitation, we considered various laboratory measurements as listed in the fourth column of Table 1. The calculated emission rates at an energy of 100 eV are close to the ones used in Roth et al. (2021), as displayed in the second and third columns of Table 1, except for electron impact on O impact leading to 135.6 nm emission for which we used different cross sections than in Roth et al. (2021). For photon impact emission excitation, we used previously published rates as indicated in Table 1.

Reactions	**Rate for electrons at 100 eV**	**Rate for electrons at 100 eV**	**Reference**

	(Roth et al. 2021)	(This work)	
$O_2 + e \rightarrow 1356$ Å	3.7×10^{-9} cm^3 s^{-1}	3.8×10^{-9} cm^3 s^{-1}	Kanik et al. (2003)
$O_2 + e \rightarrow 1304$ Å	1.57×10^{-9} cm^3 s^{-1}	1.72×10^{-9} cm^3 s^{-1}	
$O + e \rightarrow 1356$ Å	0.195×10^{-9} cm^3 s^{-1}	0.24×10^{-10} cm^3 s^{-1}	Tayal et al. (2016)
$O + e \rightarrow 1304$ Å	4.84×10^{-9} cm^3 s^{-1}	5.38×10^{-9} cm^3 s^{-1}	Johnson et al. (2005)
$H_2O + e \rightarrow 1304$ Å	0.16×10^{-9} cm^3 s^{-1}	0.19×10^{-9} cm^3 s^{-1}	Makarov et al. (2004)
$H_2O + e \rightarrow 1356$ Å	0.32×10^{-10} cm^3 s^{-1}	0.37×10^{-10} cm^3 s^{-1}	Rate at 130.4 nm divided by 5 (Roth et al. 2021)
$H_2 + e \rightarrow 1216$ Å	Not available	3.2×10^{-9} cm^3 s^{-1}	Ajello et al. (1995)
$H_2O + e \rightarrow 1216$ Å	Not available	4.2×10^{-9} cm^3 s^{-1}	Makarov et al. (2004)
Reactions	**Excitation rate**		**Reference**
$H_2O + h\nu \rightarrow H + H + O$ 1216 Å	1.4×10^{-10} s^{-1}		Roth et al. (2014)
$H + h\nu \rightarrow 1216$ Å	$7.29 – 11.8\times10^{-5}$ s^{-1}		Alday et al. (2017)
$O + h\nu \rightarrow 1304$ Å	4.0×10^{-7} s^{-1}		Roth et al. (2021)

Table 1: *Reactions and rates used to calculate the emission intensity at 1304, 1356 and 1216 Å.*

In Leblanc et al. (2017), we discussed two scenarios for the production of H_2O. One case with low sublimation rate (hereafter the dry exospheric case) is inconsistent with the H_2O/O_2 ratios from Roth et al. (2021) for O_2 column densities higher than $1x10^{13}$ cm^{-2}, as generally assumed to be the case for Ganymede (Hall et al. 1998, Johnson et al. 2004). The second case used nominal sublimation rate as calculated from Fray and Schmitt (2009) parametrization of the sublimation of water ice at very low pressure and cold temperature. Using the nominal sublimation rate scenario, we here simulate five consecutive orbits of Ganymede around Jupiter following around 2×10^6 test-particles at each time step of 0.25 s. Few hundred thousand test-particles were used to describe each of the 6 species,

namely, H, H_2, O, OH, H_2O and O_2 with weight values between 10^7 to 10^{16} (number of real particles represented by each test-particle). The macroscopic quantities like density, velocity, temperature, escape flux and reabsorbed surface flux are reconstructed on a 100 (along the radial direction) × 50 (along the polar direction) × 100 (along the azimuth direction) spherical grid. A typical run lasts one to two weeks on 64 CPUs. Four orbits are needed in order to reach a steady solution with no significant difference in the 3D reconstructed macroscopic parameters between the two last orbits.

The characteristics of the electron population at the origin of the auroral emissions remain poorly constrained by observation. Roth et al. (2021) assumed an effective averaged homogeneous electron density with values between 20 and 30 cm^{-3}, an electronic temperature of 100 eV and global O_2 abundances of ~3 x 10^{14} O_2/cm^2, which yields effective 135.6 emission brightnesses primarily produced by impact of electrons on O_2 (see Figure 3) in the range of the observed values. As discussed in Carnielli et al. (2020a), the original 10^{14} - 10^{15} O_2/cm^2 suggested by Hall et al. (1998) is based on the upper limit set by a stellar occultation observation performed by Voyager 1 (Broadfoot et al. 1979) which suggested actually an upper limit at 2.5×10^{15} cm^{-2} (Carnielli et al. 2020a). Carnielli et al. (2020a) reconstructed the ionospheric density, compared the resulting density to the G2 flyby measurements for the case of a dry exosphere (Leblanc et al. 2017) and concluded that both exospheric content and electron ionization rate might have been underestimated in previous modelling (Marconi 2007; Leblanc et al. 2017) illustrating the difficulty to derive from the auroral emission observations an accurate estimate of Ganymede's atmospheric content without knowing the electron density and temperature. Eviatar et al. (2001) using a simple auroral model (or more specifically, the electron energy spectral flux measured by Galileo over the auroral region) suggested that the electron density responsible for Ganymede's auroral emissions should be closer to a few hundred cm^{-3} rather than few ten of cm^{-3}. Such a much larger electron density would mechanically imply a much less dense exosphere in the auroral regions to explain the observed auroral brightnesses except if the electron temperature is significantly smaller than supposed by these authors.

In the following, we chose to use an electron population at 100 eV. A uniform reaction rate corresponding to the rate displayed in Table 1 multiplied by an electron density of 20 cm^{-3} is assumed everywhere except over the auroral ovals. A locally increased reaction rate is set over the latitudes ±10° of the OCFB (see Figure 3 of McGrath et al. 2013 and Figure 3 of Leblanc et al. 2017) and corresponds to the rate displayed in Table 1 multiplied by an electron density of 70 cm^{-3}. The ±10° was chosen to reproduce roughly the observed latitudinal width (c.f. Musacchio et al. 2017, their figure 9) and corresponds to the current structure in Ganymede's magnetosphere as modelled by Jia et al. (2009). The ejection mechanisms at the origin of Ganymede's exosphere are also constrained using this same separation between open and close field line regions as described in Leblanc et al. (2017).

III.2 Ganymede's exosphere as modelled by EGM

Table 2 provides the surface ejection rate for the 7 species described in EGM for the nominal sublimation rate and sputtering conditions. With the exception of water molecules which can be ejected by sublimation, most of the species are ejected from the surface by sputtering or radiolysis induced ejection. The typical rates are close to the ones used in Marconi (2007). When comparing the source rates with the neutral escape rates, we can see that loss and source terms are never equal which implies that surface reabsorption, photon and electron impact dissociation and photon and electron impact ionization are important loss mechanisms. Vorburger et al. (2021) recently published a detailed modelling of Ganymede's exosphere. They concluded that Leblanc et al. (2017) sputtering water rate was up to two orders larger than the ones of other models. It is unclear what the origin of these discrepancies is, our reconstructed yield being based on Cassidy et al. (2013) analysis derived from a large set of laboratory measurements.

Species	H	H_2	O	OH	H_2O		O_2
Source	Sputtering	Sputtering	Sputtering	Sputtering	Sputtering	Sublimation	Sputtering

Rate (s^{-1})	Surface ejection	2.0×10^{25}	8.3×10^{26}	1.0×10^{25}	1.0×10^{25}	4.0×10^{27}	8.0×10^{29}	4.4×10^{26}
	Escape	2.9×10^{26}	2.7×10^{26}	1.0×10^{26}	4.0×10^{25}	7.0×10^{26}		4.4×10^{15}

Table 2: *Simulated source and neutral escape rates (average values on 2 consecutive orbits)*

In the case of the atomic H exosphere, the neutral escape rate is 10 times larger than the sputtering rate which is due to the fact that most of the H atoms are produced from the dissociation of H_2O and H_2. Moreover, dissociation produces H atoms with enough energy to be lost by neutral escape. A small fraction of these H atoms is also reabsorbed by the surface or ionized. In the simulation, H_2 is not reabsorbed by the surface by assumption (see Leblanc et al. 2017), so that H_2 molecules either escape as neutral particle, are dissociated or are ionized. Oxygen atoms can be sputtered from the surface but are also the products of the dissociation of O_2 and H_2O. A large proportion of the O atoms are reabsorbed in the surface. In the same way, OH is either ejected from the surface by sputtering or produced from the dissociation of H_2O exospheric molecules. The main source of the H_2O exosphere is sublimation, the sputtering rate being of less than one percent of the sublimation one. Most of the H_2O molecules ejected from the surface are reabsorbed in the surface. Contrary to the other exospheric species, O_2 is too heavy to escape Ganymede gravity as neutral so that its ejection rate is balanced by the dissociation and ionization rates. Numerically, a simulation of more than 4 orbits is needed to reach a steady state between loss and source for this species.

In Figures 4 and 5, we display how Ganymede's H_2O and O_2 exospheric column densities would be seen from the Earth at the four positions of HST/STIS observations described in Figure 1. As expected and described in many past publications (see example, Marconi 2007; Plainaki et al. 2015; Leblanc et al. 2017; Plainaki et al. 2020), the H_2O exosphere is spatially organized compared to the O_2 exosphere, with a peak near the subsolar point for the H_2O whereas the O_2 column density peaks around the limb with slightly larger values near the poles. As explained in Leblanc et al. (2017), Oza et al. (2019) and Johnson et al. (2019), Ganymede's orbital motion leads to a slightly shift of the H_2O peak towards the dusk side.

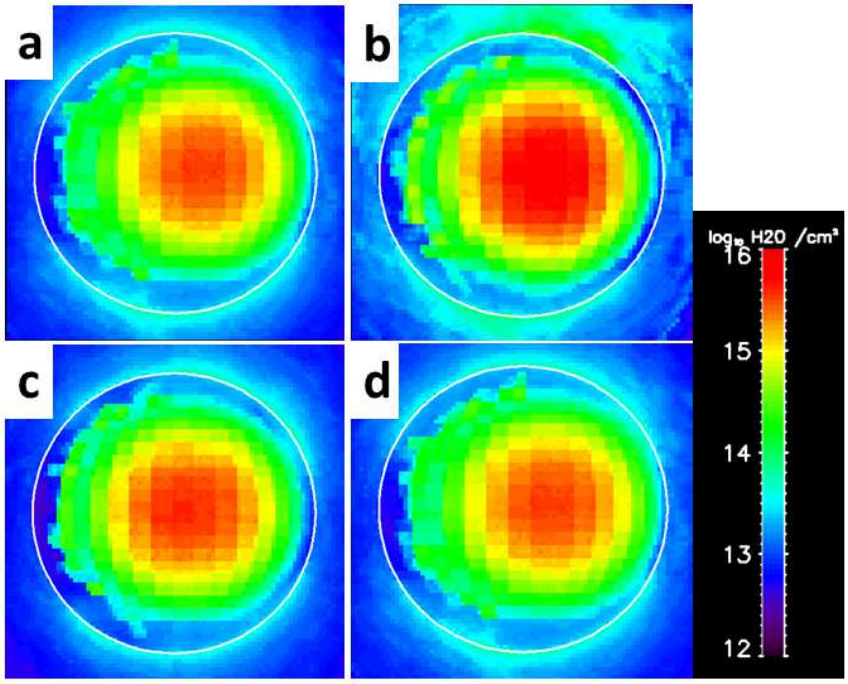

Figure 4: *Simulated column densities of the H_2O exospheric component (in log_{10} cm^{-3}) at the four positions of Figure 1 in the nominal simulation case. Panel a: phase angle of 98°-111°. Panel b: phase angle of 335°-340. Panel c: phase angle of 173° - 177°. Panel d: phase angle between 289° - 300°. The subsolar point is at the center of each panel. Dawn is on the left of each panel, the North being towards the top. Ganymede limb is represented by the white circle.*

Whereas we observe a significant change with respect to Ganymede orbital positions in the H_2O exosphere as seen from the Earth, the O_2 exosphere does not appear to vary in terms of global distribution. The water orbital variability is related to the change in surface albedo between leading and trailing sides of Ganymede (Spencer 1987) leading to a variation between 146 (maximum on the trailing side) to 142 K (minimum on the leading side) of the subsolar surface temperature and to an order of magnitude variation of the sublimation rate (see Figure 2 in Leblanc et al. 2017). The maximum H_2O column density around the subsolar region reaches values of few 10^{15} H_2O/cm^2 near the surface (and a peak density around 10^9 H_2O/cm^3 at the surface with atmospheric temperature close to the surface one up to 400 km in altitude) and decreases to a plateau at 10^{13} H_2O/cm^2 from

500 km to few thousands km in altitude (corresponding to temperature around 2000 K above 800 km). These two-slope profile is related to the two main sources of H_2O sputtering and sublimation (Table 2). The only change that can be inferred from the 2D images of the O_2 column density is due to the latitudinal extension of the polar regions which is closer to the equator when the leading side of Ganymede is illuminated (Figures 2 panels a and c) with respect to the trailing side illuminated hemisphere. The O_2 column density peaks at a value of 10^{15} O_2/cm^2 at the surface (and a density of 10^8 O_2/cm^3) and decreases by three to four orders of magnitude within the first 100 km in altitude.

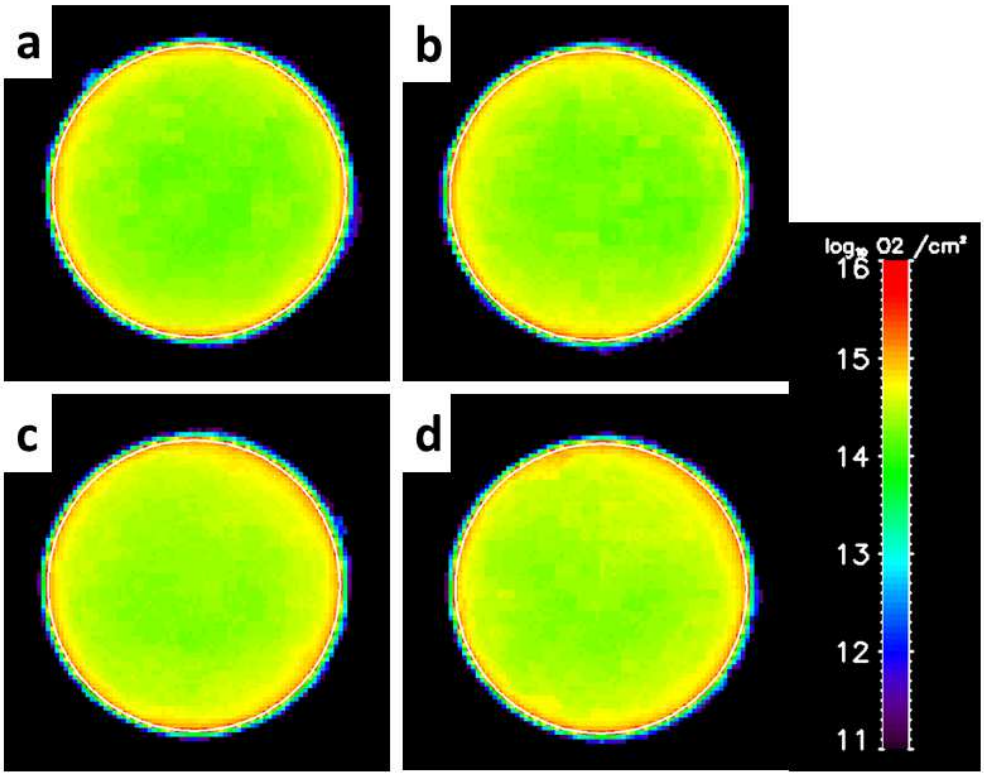

Figure 5: *Same as in Figure 4 but for the O_2 column density.*

	Phase angle 98°-111°	**Phase angle 173° - 177°**	**Phase angle 289° - 300°**	**Phase angle 335°-340°**
H	$2.5\times10^{+11}$	$1.2\times10^{+11}$	$2.8\times10^{+11}$	$2.2\times10^{+11}$
H_2	$5.6\times10^{+14}$	$6.1\times10^{+14}$	$5.0\times10^{+14}$	$4.6\times10^{+14}$
H_2O	$5.6\times10^{+14}$	$6.4\times10^{+14}$	$1.3\times10^{+15}$	$1.0\times10^{+15}$

O	$1.6\times10^{+12}$	$2.5\times10^{+12}$	$1.0\times10^{+12}$	$1.1\times10^{+12}$
O_2	$4.3\times10^{+14}$	$4.3\times10^{+14}$	$3.6\times10^{+14}$	$3.7\times10^{+14}$
OH	$1.5\times10^{+12}$	$1.5\times10^{+12}$	$1.2\times10^{+12}$	$4.7\times10^{+12}$

Table 3: *Simulated disk averaged column densities in cm^{-2} for the nominal sublimation and sputtering rate conditions*

As illustrated in Figures 4, 5 and Table 3, there is some orbital dependency of Ganymede's exosphere which are essentially driven by the leading/trailing variation of the albedo which controls the sublimation rate of the H_2O and in a lesser way the efficiency of the sputtering (Cassidy et al. 2013). Whereas the O_2 and H_2 average column densities do not change significantly along Ganymede's orbit, the H_2O exosphere column density displays a clear variation. According to Table 3, Ganymede's exosphere is always dominated by water molecules in an average over the full disk.

IV Comparison with HST observations

IV.1 Reconstructed oxygen emissions

All together, the agreement between observation and simulation using the nominal sublimation rate (section III.2) as displayed in Figure 6 is remarkably good considering that we did not make any change of the exospheric model and used a fixed temperature and density of the electrons responsible for the auroral emission (section III.1). There are however still several discrepancies between the simulated profiles (right panels in each rectangle) which could be either due to the electron population description or due to the exospheric description as discussed in the following.

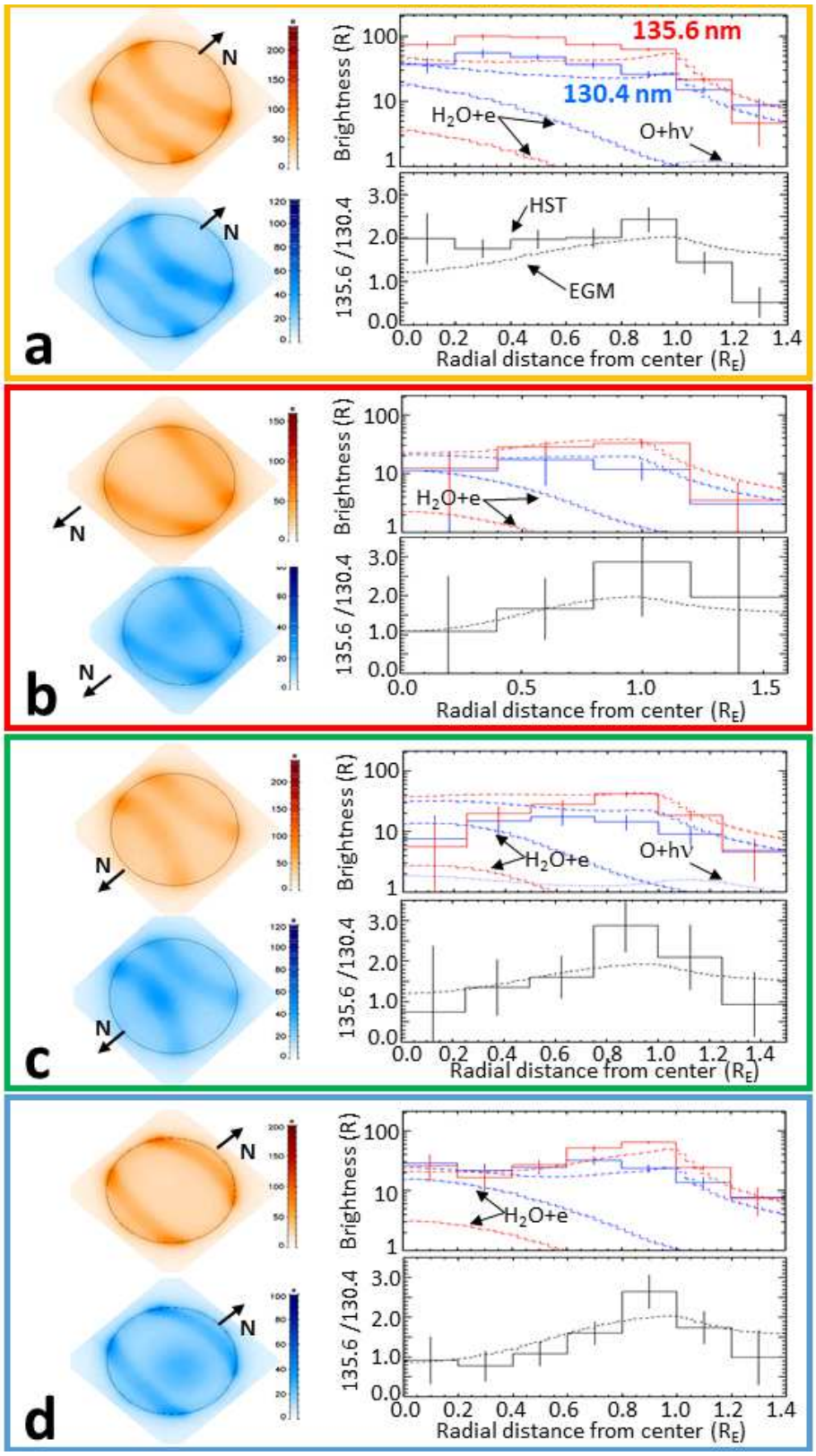

374

375 **Figure 6:** *Comparison between observation of Ganymede's atmospheric emission by HST/STIS and*

376 *EGM simulation. Each panel corresponds to one date. a 2010-11-19, phase angle of 98°-111° (Roth et*

377 *al. 2021). b: 2003-11-30, phase angle of 335°-340° (McGrath et al. 2013). c: 2017-02-02, phase angle*

of 173°-177°. d: 1998-10-30, phase angle between 289° - 300° (Roth et al. 2021). Each panel surrounded by a rectangle which colour corresponding to Figure 1 circle colours is composed of the simulated images of the 1356 A (red) and 1304 A (blue) brightness intensities, of the radial profile from the center of the disk up to around half a radius above the limb of the emission brightness intensity for these wavelength (top right panel in each rectangle with in solid line, HST/STIS observations, in dashed lines, EGM reconstructed emission intensity, in dashed-dotted lines, EGM emission intensity from H_2O+e reaction and in dotted line, EGM emission intensity from O+hν reaction) and of the ratio of these two emission lines 1356 emission intensity divided by 1304 emission intensity (bottom right panel in each rectangle).

Starting from panel a, at a phase angle of 98°-111°, that is looking to Ganymede when its leading side faces the Sun, the measured 135.6 nm emission (red solid line) is underestimated by 50% by the simulation on the disk (below a radial distance of 0.8 R_G). The observed 130.4 nm emission (solid blue line) is also slightly underestimated. The 135.6 nm emission being produced by electron impact on the O_2 molecule (the dashed-dotted red line corresponds to the emission intensity produced by electron impact on H_2O molecules which is then one order smaller), a 50% denser O_2 exosphere on the illuminated leading side or an electron density larger by 50% (that is an electron density ~100 cm^{-3} in the auroral regions) would lead to a much better reproduction of the observations close to the center of the disk. At the limb (above 1 R_G), the ratio of the two observed emission lines decreases down to a value around 0.5, showing either an increase of the amount of H_2O molecules at the origin of these emissions or an increase of the atomic oxygen abundance. Roth et al. (2021) suggested that the oxygen atoms should get more abundant in the exosphere at higher altitude being among the less massive species. Clearly, if it is the case, the model underestimates this population. Oxygen atoms can come either from the dissociation of the O_2 and H_2O or directly from the surface sputtering. Since increasing the O_2 and H_2O densities, in particular close to the limb, would lead to a

discrepancy with the observations, the most plausible explanation is that the flux of O atoms sputtered from the surface is underestimated by the model. We therefore tested much larger ejection rate by sputtering of the O atoms, by up to a factor 100, and simulated an exosphere with emissions closer to the ones reported in Figure 2 but still not matching the observed emission brightness ratio at 1.3 R_G from the limb. The reconstructed 2D images of the emission brightness as displayed in Figure 6a (left) reproduced the shape of the auroral emissions, logically since we imposed it arbitrarily in our reconstruction of these emissions, through the increase in electron density around the OCBF (see section III). We also simulated a limb asymmetry between dawn and dusk, an asymmetry due to the asymmetry of the exosphere as seen from the Earth. Such asymmetry in the auroral emissions might be also related to the electron current system as discussed by Musacchio et al. (2017).

At a phase angle around 335° - 340° (panel b in Figure 6), the Sub-Jovian hemisphere of Ganymede faces the observer. For such case, the model results are in rather good agreement with the observation, the emission brightness intensities of the two emission lines and their ratio being reproduced by the model within the uncertainties of the observation. A similar excellent agreement between simulation and observation is also obtained at a phase angle of 289°-300° (panel d). However, at 0.9 R_G from the center of the disk, the observed ratio reaches a value above 2.5. Even with a pure O_2 exosphere, maximum values around 2 would be produced according to Figure 3d, making a ratio of 2.5 very unlikely with only a mixture of H_2O and O_2.

The comparison between simulated emission brightness intensity and observed ones in panel c (phase angle of 173° - 177°) displays significant discrepancies. Close to the center of the disk, the model calculated an emission brightness much more intense than observed, by a factor 6 for the 135.6 nm emission and a factor 4 for the 130.4 nm emission. At this orbital position, Ganymede's anti-Jovian hemisphere faces the observer. A potential reason for the observed decrease in the emission brightness intensity close to the center of the disk at such orbital position might be

428 therefore related to the dependency of the current system at the origin of these auroral emissions
429 with respect to the ram/wake orientation and Jovian/Anti-Jovian hemisphere, a dependency that we
430 did not consider when adopting constant density and energy of the electron in the auroral bands. A
431 smaller density of the electron at the origin of these emissions would lead to a less intense emission
432 intensity but to a similar value of their ratio. At the limb, the observed emission lines have similar
433 intensities, leading to a ratio close to one. The simulation predicts a ratio close to 1.5 which is
434 consistent with the observation when considering the uncertainty on the observed ratio. At 0.8 R_G
435 from the center of the apparent disk, this same ratio reaches a value of 2.8±0.7. If real, it would
436 suggest a mechanism for the production of these emissions which is not taken into account in our
437 model.

438 To summarize, the nominal sublimation model of Ganymede's exosphere convolved with the simple
439 description of the population of electron at the origin of the observed emission leads to a good
440 agreement with the observation on the side of the orbit when Ganymede trailing hemisphere is
441 facing the Sun. We obtained a less good agreement on the other side. In the exospheric model, the
442 only difference taken into account between these two portions of the orbit is related to the change
443 of the wake/ram angle with respect to the subsolar/anti-solar direction. The most probable origin of
444 this discrepancy is related to the simple description of the electron population leading to these
445 auroral emissions. This population has been shown to be variable and dependent on the wake/ram,
446 Sub-solar – anti-jovian axis and to the sub-solar direction (Jia et al. 2009; Sauer et al. 2015). As a
447 matter of fact, Carnielli et al. (2020a) reconstructed the ionosphere of Ganymede using Leblanc et al.
448 (2017) dry exospheric model and concluded that the density of ionising electrons is denser than
449 previously inferred from Galileo (Carnielli et al. 2019) at (or extrapolated to) Ganymede's orbit so
450 that the electron impact ionization frequency should be increased by a factor 4 in the anti-Jovian
451 hemisphere for the G2 flyby conditions. As a matter of fact, recent radio-occultation observations
452 performed during JUNO flyby of Ganymede suggest an electron density close to the surface of
453 2000±500 cm^{-3} in the open magnetic field regions of Ganymede magnetosphere (Buccino et al.

2022). A higher ionisation frequency is also consistent with our conclusions that to reproduce the observed emission profiles above the limb, a higher electron impact dissociation rate of O_2 is needed. Carnielli et al. (2020a) also concluded that the O_2 density in the polar regions should be increased by a factor 10 with respect to the dry scenario (Table 3). The nominal sublimation scenario used here leads to H_2O average column densities 30 to 100 times denser than in the dry scenario (Leblanc et al. 2017). However, a nominal sublimation rate scenario might be not enough to reproduce Galileo electron density at high latitudes, since the H_2O exosphere is essentially concentrated in the sublimation equatorward region. Moreover, a 10 times denser O_2 exosphere convolved with a higher electron impact rate, would probably lead to a significantly larger 135.6 nm / 130.4 nm ratio in the auroral regions in disagreement with the observations (Figure 6). Without a detailed knowledge of the electron density and temperature in the open field lines regions, it is therefore not realistic to conclude firmly on how to reconcile measured electron density and auroral emission intensities. We note, however, that the 135.6 nm / 130.4 nm ratio for O_2 is similar within the relevant electron temperatures range (e.g. Kanik et al. 2003 and Figure 3d). If the ratio for H_2O is similarly insensitive to the temperature as supposed in Figure 3d, firm conclusions are possible without exact knowledge of the absolute excitation and brightnesses.

As discussed before, the ratio of the two measured emission lines above the limb suggests an underestimate of the O population by EGM in this region. We simulated much larger sputtering rate of the O atoms (by a factor 100) from the surface without changing significantly the simulated ratio displayed in Figure 6. The main reason is that the main source of the O exospheric population is not its sputtering from the surface but the dissociation of O_2 and H_2O. We therefore performed a simulation with an electron impact rate increased by a factor 2.0 in the open field lines region (equivalent to increase the electron density by a similar factor). However, increasing the electron impact dissociation also leads to a lower density of both molecules and therefore a smaller brightness intensity at 130.4 and 136.6 nm. We had therefore to increase by a factor 1.8 the sputtering rate of both O_2 and H_2O to compensate the increase in their dissociation rate to fit the

observed emission brightness. We also had to increase the sputtering rate for O and H with respect to the one of O_2 by a factor 40 in order to retrieve emission brightness ratio above the limb close to the ones observed by HST. With such increase of the sputtering rate of H and O, sputtering is equivalent to the dissociation of O_2 and H_2 as source for these two exospheric species. The density for these two species significantly increased by more than an order of magnitude in the case of H and by a factor 2 to 3 in the case of the O exosphere. In that case, the simulated O column density is marginally larger than the upper limit set by Roth et al. (2021) for the column density by a factor 2.5. The other species, namely H_2, O_2, H_2O and OH, remains almost unchanged with respect to the nominal species.

IV.2 Reconstructed H emission

Lyman α emission from Ganymede's atmosphere was detected for the first time by Galileo (Barth et al. 1997) and later confirmed from HST by Feldman et al. (2000). Recently, Alday et al. (2017) provided a detailed analysis of four sets of HST observations obtained between 1998 and 2014. These authors estimated the emission brightness from Ganymede's corona (outside from the apparent disk) as ranging from 0 to 450 R for a phase angle between 77.9° and 103.5° (average emission of 215±66 R), from 110 to 310 R for a phase angle between 269.3° and 291.8° (average emission of 180±52 R). As discussed in Alday et al. (2017), the globally lower emission intensities of the Lyman α emission obtained in 2014 with respect to the other set of observations obtained in 1998, 2010 and 2011 are probably due to strong absorption of the emission by the geocorona. Excluding these 2014 observations, the Lyman α emission brightness between 90.1° and 103.5° is 328±159 R and at 291.8° is 310 R.

In order to predict brightnesses, we simulated the emission brightness at Lyman α using the various possible excitation processes described in Table 1 for the nominal exosphere case. At a phase angle of 98° - 111°, the emission brightness intensity at Lyman α was simulated as being equal to 170

505 Rayleigh on the apparent disk and 47 Rayleigh outside. On the disk, H_2O electron impact emission
506 dominates with 100 Rayleigh induced by this process and 50 Rayleigh is associated with H_2 electron
507 impact. Outside of the disk, H_2O electron impact induces only 9 Rayleigh of emission intensity and 25
508 Rayleigh is produced by H_2 electron impact. Very similar values are simulated at a phase angle of 289°
509 - 300°. These H Lyman-alpha aurora intensities are not discernible from the other sources in the HST
510 observations and therefore not detectable. For resonant scattering by H atoms, we get intensities on
511 the order of 10-20 Rayleigh for our simulations. With respect to the reported emission intensity in
512 the extended corona outside of the disk with peak brightness near the moon of ~300 R (Alday et al.
513 2017), our simulated intensities are therefore an order of magnitude too low.

514 The only way to increase the simulated emission intensity would be to increase the density in H
515 atoms. exospheric H atoms are produced either from direct sputtering from the surface or coming
516 from the dissociation of H_2O and H_2. Increasing the H_2O or H_2 dissociation rate is possible by
517 increasing the H_2O or H_2 density but this would lead to a disagreement between simulation and
518 observation regarding the OI 130.4 nm and 135.6 nm emission line profiles (Figure 6). It is also
519 possible that the dissociation frequency used in our simulation for these two molecules is
520 underestimated because of a higher electron density or temperature. Increasing the electron energy
521 would lead to a small increase of the electron impact dissociation, the typical electron impact
522 dissociation cross section with respect to the electron energy forming a plateau above 20 eV for H_2+e
523 $\rightarrow$ H + H (Dalgarno et al. 1999) or peaking around 100 eV for H_2O+e $\rightarrow$ H+OH and H_2O + e $\rightarrow$ H+H+O
524 (Song et al. 2021). We performed a simulation where the electron impact rate is increased by a factor
525 2 through an increase of the electron density in the open field lines region, combined with a
526 sputtering rate of the H atoms increased by a factor 72. In that case, between 98° and 111°, the H
527 density in the corona of Ganymede is increased by a factor 10, leading to a stronger emission
528 intensity from the corona equal to 450 Rayleigh on the disk and of 230 Rayleigh outside the disk
529 (with 20 Rayleigh produced by electron impact on H_2 and 200 by resonant scattering on H atoms). At
530 a phase angle of 289° - 300°, the H corona is also increased by a factor 10 leading to an emission

brightness of 300 Rayleigh on the disk and of 180 Rayleigh outside the disk (with 20 Rayleigh produced by electron impact on H_2 and 160 by resonant scattering on H atoms). Therefore, as concluded in the case of the oxygen atoms, a sputtering rate of H atoms from Ganymede surface increased by almost two orders of magnitude and a factor two increase of the electron impact dissociation of H_2 and H_2O with respect to the nominal value are needed to reproduce the brightness intensity of the Lyman α extended exosphere of Ganymede.

VI Conclusion

Ganymede's atmosphere is thought to be composed of water molecules and its products (in particular O_2), thanks to several set of observations from Galileo and Hubble Space Telescope (HST) and to modelling (see Roth et al. 2021 for more details). Ganymede's atmosphere is probably unique in our solar system, in the sense, that it is not exactly a surface bounded exosphere as defined by Stern (1999) but is probably collisional locally. Indeed, it is partly produced by (1) the sublimation of its icy surface around the subsolar point which leads to a water molecular atmosphere locally thick enough to be collisional; and (2) for the rest of its surface, by the permanent bombardment of its surface by the Jovian and ionospheric electrons and ions leading to radiolysis and sputtering (Roth et al. 2021). The observation of Ganymede's atmosphere presented in Roth et al. (2021) provided for the first time the clear evidence of the presence of a thick water molecular atmospheric component as predicted by Marconi (2007). Roth et al. (2021) analysed a set of HST observations with a simple parametric description of Ganymede's atmosphere and derived the amount of water molecule that should be present around Ganymede. A recent study by de Kleer et al. (2023) measured optical oxygen emissions deriving a global upper limit on the H_2O/O_2 ratio below Roth et al. (2021) derived ratios from aperture-integrated emissions brightnesses. Although the authors claim a conflict with Roth et al. (2021) results, they are in fact consistent: the majority of the emissions on the sub-Jovian are located near or above the limb. The globally integrated emission ratio, which de Kleer et al. use,

556 is therefore only representative for this region and the lower line ratio on the disk center and the
557 H_2O abundance there will remain undetected in their data.

558 In this paper, the newly published observations are taken such that the anti-Jovian and sub-Jovian
559 hemispheres are observed, i.e. at intermediate geometries between the previously published leading
560 and trailing side observations (Roth et al. 2021). The new data show that the 135.6 nm/130.4 nm
561 ratio in the Ganymede disk center is also intermediate, i.e., lower on the leading side but higher on
562 the trailing side. This means that the oxygen emission ratio and related molecular abundances
563 appear to be modulated by Ganymede's orbital period. Using a simplified description for the electron
564 to reconstruct the electron impact excitation at the origin of HST observations, we showed that
565 Exospheric Global Model (EGM; Leblanc et al. 2017) provides a rather good agreement with this set
566 of observations obtained at four positions of Ganymede around its orbit. By modelling the orbital
567 variability of the surface radiolysis and sublimation and their dependency with respect to the intrinsic
568 Ganymede's magnetosphere and to the surface temperature, EGM succeeded to provide a
569 consistent description of the origins of Ganymede's exosphere and of its content.

570 We found slightly smaller amount of water than Roth et al. (2021), with an average disk column
571 density between $0.5\times10^{+15}$ H_2O/cm^2 when the leading hemisphere of Ganymede is illuminated and
572 $1.3\times10^{+15}$ when it is the trailing hemisphere. The H_2O atmosphere density on the sub-Jovian and anti-
573 Jovian sides is in between these values, consistent with the observations. The O_2 atmosphere is less
574 variable with an average disk column density around $4.0\times10^{+14}$ O_2/cm^2, a relatively low abundance
575 with respect to previous analysis (Hall et al. 1998). Our analysis also suggests that the spatial
576 distribution of the exosphere should be slightly shifted towards the dusk side on the dayside, in
577 particular for its H_2O component. We also discussed the reconstructed Lyman α emission brightness
578 and compared it to observations (Alday et al. 2017) and showed that the model significantly
579 underestimates the brightness intensity of this emission line far from Ganymede's surface. As for the
580 oxygen emission lines, we concluded that to reproduce the emission brightness far from the surface,

a much higher sputtering rate of the oxygen and hydrogen atoms is needed with respect to the nominal rate used in Leblanc et al. (2017) and previous publications. This higher sputtering rate should be also combined with a two times higher dissociation rate of the exospheric molecules close to Ganymede, suggesting a denser electron population with enough energy to dissociate the exospheric molecules in the open field line regions than supposed in Leblanc et al. (2017).

This paper provides the first consistent attempt to reconstruct of the observations that presently constrain Ganymede's exosphere. It also highlights the need to properly take into account the various possible sources of the auroral emissions, in particular the electron population. Without either in-situ measurements to better constrain this electron population, or detailed modelling of the ionosphere and its suprathermal electron component, any analysis of the auroral emissions observed around Ganymede would remain a degenerated problem. Other methods to observe Ganymede's atmosphere are therefore highly needed to resolve this non-constrained issue.

Acknowledgement: F.L., R.M. and J.-Y.C. acknowledge the support by ANR of the TEMPETE project (grant ANR-17-CE31-0016). Authors are also indebted to the "Système Solaire" and "Soleil Héliosphère et Magnétosphère" programs of the French Space Agency CNES for their supports. Work at Imperial College London was supported by the STFC of the UK under grant ST/W001071/1. Authors also acknowledge the support of the IPSL data center CICLAD for providing us access to their computing resources and data. Data may be obtained upon request from F. Leblanc (email:francois.leblanc@latmos.ipsl.fr).

602
603 **References**

604 Ajello J.M., Kanik I., Ahmed S.M. and J.T. Clarke, Line profile of H Lyman α from dissociative excitation
605 of H_2 with application to Jupiter, J. Geophys. Res. et al., 100, E12, 26411-26420, 1995

606 Alday J., L. Roth, N. Ivchenko, K. D. Retherford, T. M. Becker, P. Molyneux, and J. Saur. New
607 constraints on Ganymede's hydrogen corona: Analysis of Lyman-_ emissions observed by HST/STIS
608 between 1998 and 2014. Planet. Space Sci., 148:35-44, Nov 2017. doi: 10.1016/j.pss.2017.10.006.

609 Barth, C.A., Hord, C.W., Stewart, A.I.F., Pryor, W.R., Simmons, K.E., McClintock, W.E., Ajello, J.M.,
610 Naviaux, K.L. and Aiello, J.J.: Galileo ultraviolet spectrometer observations of atomic hydrogen in the
611 atmosphere of Ganymede, Geophys. Res. Lett., 24, 2147–2150, 1997

612 Broadfoot A. L., Belton M. J., Takacs P. Z., Sandel B. R., Shemansky D. E., Holberg J. B., Ajello J. M.,
613 Moos H. W., Atreya S. K., Donahue T. M., Bertaux J. L., Blamont J. E., Strobel D. F., McConnell J. C.,
614 Goody R., Dalgarno A., and McElroy M. B. Extreme ultraviolet observations from Voyager 1
615 encounter with Jupiter. Science, 204:979–982, June 1979. doi: 10.1126/science.204.4396.979. URL
616 http://adsabs.harvard.edu/abs/1979Sci...204..979B.

617 Buccino D.R., Parisi M., Gramigna E., Gomez-Casajus L., Tortora P., Zannoni M., Caruso A., Park R.S.,
618 Withers P., Steffess P., Hodges A., Levin S. and Bolton S., Ganymede's Ionosphere observed by a Dual-
619 Frequency Radio Occultation with Juno, Geophys. Res. Let, 2022. doi: 10.1029/2022GL098420.

620 Carnielli G., Galand M. Leblanc F., L. Leclercq, Modolo R. and A. Beth, First 3D test particle
621 model of Ganymede's ionosphere, Icarus, 330, 42, 2019. ⟨10.1016/j.icarus.2019.04.016⟩ - insu-
622 02111422

623 Carnielli G., M. Galand, F. Leblanc, R. Modolo, A. Beth, X. Jia, Constraining Ganymede's neutral and
624 plasma environments through simulations of its ionosphere and Galileo observations, Icarus, 343,
625 113691, 2020a. ⟨10.1016/j.icarus.2020.113691⟩

626 Carnielli G., M. Galand, F. Leblanc, R. Modolo, A. Beth, X. Jia, Simulations of ion sputtering at
627 Ganymede, Icarus, Icarus, 351, 113918, 2020b. ⟨10.1016/j.icarus.2020.113918⟩

628 Cassidy T.A., C.P. Paranicas, J.H. Shirley, J.B. Dalton III, B.D. Teolis, R.E. Johnson, L. Kamp, A.R.
629 Hendrix, Magnetospheric ion sputtering and water ice grain size at Europa. Planet. Space Sci. **77**, 64–
630 73 (2013). https://doi.org/10.1016/j.pss.2012.07.008

631 Cooper J.F., R. E. Johnson, B. H. Mauk, H. B. Garrett, and N. Gehrels. Energetic Ion and Electron
632 Irradiation of the Icy Galilean Satellites. Icarus, 149(1):133-159, 2001. doi: 10.1006/icar.2000.6498.

633 Dalgarno A., Yan M., W. Liu, Electron energy deposition in a gas mixture of atomic and molecular
634 hydrogen and helium, ApJS, 125:237-256, 1999. 10.1086/313267

635 de Kleer K., Milby Z., Schmidt C., Camarca M. and M. Brown, The Optical Aurorae of Europa,
636 Ganymede and Callisto, The Planetary Science Journal, 4:37, 2023.
637 https://doi.org/10.3847/PSJ/acb53c

638 Feldman, P.D., McGrath, M.A., Strobel, D.F., Warren Moos, H., Retherford, K.D., Wolven, B.C.,
639 HST/STIS ultraviolet imaging of polar aurora on Ganymede. Astrophys. J. 535, 1085–1090, 2000.

640 Fray, N., Schmitt, B., Sublimation of ices of astrophysical interest: A bibliographic review. Planet.
641 Space Sci. 57, 2053–2080, http://dx.doi.org/10.1016/j.pss.2009.09.011, 2009.

642 Hall, D.T., Feldman, P.D., McGrath, M.A., Strobel, D.F., The far-ultraviolet oxygen airglow of Europa
643 and Ganymede, The Astrophysical Journal 499, 475, 1998.

644 Jia, X., Walker, R.J., Kivelson, M.G., Khurana, K.K., Linker, J.A., 2009. Properties of Ganymede's
645 magnetosphere inferred from improved three-dimensional MHD simulations. Journal of Geophysical
646 Research (Space Physics) 114, A09209. URL: http://adsabs.harvard.edu/abs/2009JGRA..114.9209J,
647 doi:https://doi.org/10.10 29/2009JA014375.

Johnson P.V., J.W. McConkey, S.S. Tayal, and I. Kanik, Collisions of electrons with atomic oxygen: current status, Can. J. Phys. 83: 589–616, 2005, doi: 10.1139/P05-034

Johnson, R.E., Carlson, R.W., Cooper, J.F., Paranicas, C., Moore, M.H.,Wong, M.C., 2004. In: Bagenal, F., Dowling, T., McKinnon, W. (Eds.), Jupiter Atmosphere, Satellites and Magnetosphere. Cambridge Univ. Press, Cambridge, UK, pp. 485–512.

Johnson, R.E., A.V. Oza, F. Leblanc, C. Schmidt, T.A. Nordheim, The Origin and Fate of O2 in Europa's Ice: an Atmospheric Perspective, Space Science Review, 215, 1, 2019. ⟨10.1007/s11214-019-0582-1⟩ - insu-02020077

Kanik I., C. Noren, 489 O. P. Makarov, P. Vatti Palle, J. M. Ajello, and D. E. Shemansky. Electron impact dissociative excitation of O2: 2. Absolute emission cross sections of the OI(130.4 nm) and OI(135.6 nm) lines. J. Geophys. Res., 108:5126, 2003.

Leblanc F., Leclercq L., A. Oza, C. Schmidt, Modolo R., J.Y. Chaufray and R.E. Johnson, On the orbital variability of Ganymede's atmosphere Icarus, 293, 185-198, doi: 10.1016/j.icarus.2017.04.025, 2017.

Makarov, O. P., J. M. Ajello, P. Vattipalle, I. Kanik, M. C. Festou, and A. Bhardwaj, Kinetic energy distributions and line profile measurements of dissociation products of water upon electron impact, J. Geophys. Res., 109, A09303, doi:10.1029/2002JA009353, 2004

Marconi, M.L., A kinetic model of Ganymede’s atmosphere. Icarus 190, 155– 174, 2007.

Marzok, A., Schlegel, S., Saur, J., Roth, L., Grodent, D., Strobel, D. F., & Retherford, K. D. (2022). Mapping the brightness of Ganymede's ultraviolet aurora using Hubble Space Telescope observations. *Journal of Geophysical Research: Planets*, *127*, e2022JE007256. https://doi.org/10.1029/2022JE007256

McClintock W. E., G. J. Rottman, and T. N. Woods. Solar-Stellar Irradiance Comparison Experiment II (Solstice II): Instrument Concept and Design. Sol. Phys., 230:225-258, 2005.

671 McGrath, M.A., Xianzhe, J., Retherford, K., Feldman, P.D., Stroberl, D.F., Saur, J., Aurora on
672 Ganymede. J. Geophys. Res.: Space Phys. 118 (5), 2043–2054, 2013.

673 Modolo R., S. Hess, M. Mancini, F. Leblanc, JY Chaufray, D. Brain, L. Leclercq, G. Chanteur, P. Weill,
674 Gonzalez-Galindo, F. Forget, M. Yagi and C. Mazelle, Mars-solar wind interaction: LatHyS, an
675 improved parallel 3D multi-species hybrid model, J. Geophys. Res., 121 (7), 6378-6399, 2016.

676 Molyneux P. M., J. D. Nichols, N. P. Bannister, E. J. Bunce, J. T. Clarke, S. W. H. Cowley, J. C. Gérard, D.
677 Grodent, S. E. Milan, and C. Paty. Hubble Space Telescope Observations of Variations in Ganymede's
678 Oxygen Atmosphere and Aurora. Journal of Geophysical Research (Space Physics), 123(5):3777-3793,
679 2018. doi: 10.1029/2018JA025243.

680 Musacchio, F., J. Saur, L. Roth, K. D. Retherford, M. A. McGrath, P. D. Feldman, and D. F. Strobel
681 (2017), Morphology of Ganymede's FUV auroral ovals, *J. Geophys. Res. Space Physics*, *122*, 2855–
682 2876, doi:10.1002/2016JA023220.

683 Neubauer, F.M., The sub-Alfvnic interaction of the Galilean satellites with the Jovian magnetosphere.
684 Journal of Geophysical Research 104 (E2), 3863, 1999. http://doi.wiley.com/10.1029/1998JE900031

685 Oren M. and Nayar S. K., Generalization of Lambert's Reflectance Model, Proceedings of the 21st
686 Annual Conference on Computer Graphics and Interactive Techniques: 239–246, 1994.
687 *doi*:*10.1145/192161.192213*

688 Oza A. V., F. Leblanc, R. E. Johnson, C. Schmidt, L. Leclercq, Cassidy T. and J.Y. Chaufray, Dusk over
689 dawn O_2 asymmetry in Europa's near-surface atmosphere, Planetary & Space Science, 167, 23-32,
690 2019. doi.org/10.1016/j.pss.2019.01.006

691 Plainaki, C., Milillo, A. , Massetti, S. , Mura, A., Jia, X., Orsini, S., Mangano, V., DeAngelis, E., Rispoli, R.,
692 The H_2O and O_2 exospheres of Ganymede: the result of a complex interaction between the jovian
693 magnetospheric ions and the icy moon, Icarus, 245, 306–319,
694 http://dx.doi.org/10.1016/j.icarus.2014.09.018, 2015.

Plainaki C., G. Sindoni, D. Grassi, L. Cafarelli, E. D'Aversa, S. Massetti, A. Mura, A. Milillo, G. Filacchione, G. Piccioni, Y. Langevin, F. Poulet, F. Tosi, A. Migliorini, and F. Altieri. Preliminary estimation of the detection possibilities of Ganymede's water vapor environment with MAJIS. Planet. Space Sci., 191:105004, 2020a, doi: 10.1016/j.pss.2020.105004.

Plainaki C., S. Massetti, X. Jia, A. Mura, A. Milillo, D. Grassi, G. Sindoni, E. D'Aversa, and G. Filacchione. Kinetic Simulations of the Jovian Energetic Ion Circulation around Ganymede. ApJ, 900(1):74, 2020a. doi: 10.3847/1538-4357/aba94c.

Roth L., J. Saur, K. D. Retherford, P. D. Feldman, and D. F. Strobel. A phenomenological model of Io's UV aurora based on HST/STIS observations. Icarus, 228:386-406, 2014.

Roth L., J. Saur, K. D. Retherford, D. F. Strobel, P. D. Feldman, M. A. McGrath, J. R. Spencer, A. Blöcker, and N. Ivchenko. Europa's far ultraviolet oxygen aurora from a comprehensive set of HST observations. Journal of Geophysical Research (Space Physics), 121:2143-2170, March 2016.

Roth L. et al., Evidence for a sublimated water atmosphere on Ganymede from Hubble Space Telescope Observations, Nature, 2021

Roth L., C. Plainaki, A.V. Oza, A. Vorburger, R.E. Johnson, P.M. Moyneux, K.D. Retherford, F. Leblanc, S. Massetti, A. Mura and P. Wurz, Ganymede's tenuous atmosphere, Ganymede book, 2022

Roth L., Marchesini G., Becker T.M., Hoeijmakers H.J., Molyneux, P.M., Retherford K.D., Saur J., Carberry Mogan S.R. and J.R. Szalay, Probing Ganymede's Atmosphere with HST Lyα Images in Transit of Jupiter, The Planetary Science Journal, 4:12, 2023. https//doi.org/10.3847/PSJ/acaf7f

Saur, J., Duling, S., Roth, L., Jia, X., Strobel, D. F., Feldman, P. D., et al. (2015). The search for a subsurface ocean in Ganymede with Hubble Space Telescope observations of its auroral ovals. *Journal of Geophysical Research: Space Physics*, *120*(3), 1715–1737. https://doi.org/10.1002/2014JA020778

718 Shemansky D.E., Yung Y.L., Liu W., Yoshii J., Hansen C.J., Hendrix A.R. and L.W. Esposito, A new
719 understanding of the Europa Atmosphere and limits on geophysical activity, ApJ, 797-84, 2014. doi:
720 10.1088/0004-637X/797/2/84

721 Shematovich, V.I., Neutral Atmosphere Near the Icy Surface of Jupiter's Moon Ganymede, Solar
722 System Research, 2016, 50, 4, 262–280, 2016.

723 Song M.Y., Hyuck C., Karwasz G.P., Kokoouline V., Nakamura Y., Tennyson J., Faure A., Mason N.J. and
724 Y. Itikawa, J. Phys. Chem. Ref. Data 50, 023103 (2021). doi: 10.1063/5.0035315

725 Spencer, J.R., Icy Galilean satellite reflectance spectra: less ice on Ganymede and Callisto? Icarus 70,
726 99–110, 1987.

727 Spencer J. R., L. A. Lebofsky, and M. V. Sykes. Systematic biases in radiometric diameter
728 determinations. Icarus, 78(2):337{354, 1989. doi: 10.1016/0019-1035(89)90182-6.

729 Stern, S.A., The lunar atmosphere: history, status, current problems and context, Reviews of
730 Geophysics, 37, 4, 453–491, 1999.

731 Tayal S.S. and O. Zatsarinny, *B*-spline *R*-matrix-with-pseudostates approach for excitation and
732 ionization of atomic oxygen by electron collisions, Physical Review A 94, 042707, 2016. doi:
733 10.1103/PhysRevA.94.042707

734 Turc, L., Leclercq, L., Leblanc, F., Modolo, R., Chaufray, J.-Y., Modelling Ganymede's neutral
735 environment: A 3D test-particle simulation. Icarus 229, 157–169, 2014.

736 Vasyliūnas V.M. and A. Eviatar, Outflow of ions from Ganymede: a reinterpretation, Geophys. Res.
737 Let., 27, 9, 1347-1349, 2000.

738 Vorburger A., Fatemi S., Galli A., Liuzzo L., Poppe A.R. and P. Wurz, 3D Monte-Carlo simulation of
739 Ganymede's water exosphere, Icarus, 375, 114810, 2022.
740 https://doi.org/10.1016/j.icarus.2021.114810